Published online 4 December 2019

Nucleic Acids Research, 2020, Vol. 48, No. 2 ***517–532***
doi: 10.1093/nar/gkz1136

Inhibition of histone deacetylase 1 (HDAC1) and HDAC2 enhances CRISPR/Cas9 genome editing

Bin Liu[1,*,†], Siwei Chen[1,†], Anouk La Rose[1], Deng Chen[1], Fangyuan Cao[1], Martijn Zwinderman[1], Dominik Kiemel[1,2], Manon Aïssi[1], Frank J. Dekker[1] and Hidde J. Haisma[1,*]

[1]Department of Chemical and Pharmaceutical Biology, Groningen Research Institute of Pharmacy, University of Groningen, Groningen 9713 AV, The Netherlands and [2]Department of Infectious Diseases, Molecular Virology, University of Heidelberg, Heidelberg, 69120, Germany

Received June 28, 2019; Revised November 18, 2019; Editorial Decision November 19, 2019; Accepted November 21, 2019

ABSTRACT

Despite the rapid development of CRISPR/Cas9-mediated gene editing technology, the gene editing potential of CRISPR/Cas9 is hampered by low efficiency, especially for clinical applications. One of the major challenges is that chromatin compaction inevitably limits the Cas9 protein access to the target DNA. However, chromatin compaction is precisely regulated by histone acetylation and deacetylation. To overcome these challenges, we have comprehensively assessed the impacts of histone modifiers such as HDAC (1–9) inhibitors and HAT (p300/CBP, Tip60 and MOZ) inhibitors, on CRISPR/Cas9 mediated gene editing efficiency. Our findings demonstrate that attenuation of HDAC1, HDAC2 activity, but not other HDACs, enhances CRISPR/Cas9-mediated gene knockout frequencies by NHEJ as well as gene knock-in by HDR. Conversely, inhibition of HDAC3 decreases gene editing frequencies. Furthermore, our study showed that attenuation of HDAC1, HDAC2 activity leads to an open chromatin state, facilitates Cas9 access and binding to the targeted DNA and increases the gene editing frequencies. This approach can be applied to other nucleases, such as ZFN and TALEN.

INTRODUCTION

CRISPR/Cas9 (clustered regularly interspaced short palindromic repeats/CRISPR-associated protein 9) is derived from the bacterial immune system where it disrupts foreign genetic elements invaded from plasmids and phages, which are eventually naked DNA. Nowadays, it is widely used in genome editing for eukaryotes, including humans (1–5). However, the eukaryotic chromosomes are more complex than their prokaryotic counterparts. In eukaryotes, DNA is packed into chromosomes in the cell nucleus in a highly compact and organized manner named chromatin. The chromatin is made up of repeating units called nucleosomes. The nucleosome consists of 147 bp wrapped around histone protein octamers H2A, H2B, H3 and H4 (6). Thus, the gene editing process of CRISPR/Cas9 in eukaryotes is very different as compared to the prokaryotic process.

CRISPR/Cas9 system is revolutionizing the field of biochemical research, but a higher efficiency is anticipated for clinical practice. The efficiency of genome editing by CRISPR/Cas9 varies from 2% to ∼25% depending on the cell type (7), which is not yet up to the requirements for clinical use, such as cancer gene therapy (8). Most approaches for optimizing CRISPR based techniques are mainly focused on optimizing the structure of gRNAs (9–11), creating mutant Cas9 (12) and finding new versions of CRISPR/Cas system from prokaryotes (13–16), etc. Although these approaches are essential, the underlying genomic context, particularly the chromatin state of the target locus, significantly influences the cleavage efficiency (17,18). Recent studies showed that the targeting efficiency of CRISPR/Cas9 varied widely in different target loci of the chromosome (18,19). The euchromatic target sites show higher frequencies of DSB (double-strand break) introduced by TALENs and CRISPR/Cas9 as compared to those of the heterochromatic sites. Notably, a recent study showed that the spontaneous breathing of nucleosomal DNA and chromatin remodelling facilitates Cas9 to effectively act on chromatin (20). Thus, the chromatin conformations can significantly impact gene editing efficiency of nucleases.

*To whom correspondence should be addressed. Email: bin.liu@rug.nl
Correspondence may also be addressed to H.J. Haisma. Tel: +31 50 363 8174; Fax: +31 50 363 3247; Email: h.j.haisma@rug.nl
†The authors wish it to be known that, in their opinion, the first two authors should be regarded as joint First Authors.

Undoubtedly, there is a considerable number of target sites inevitably located in heterochromatin, which has a strong effect on the accessibility of DNA to Cas9 (21). Furthermore, albeit many genes are located in a relatively euchromatic position, the gene editing efficiency may also be enhanced through maintaining the open state of those euchromatic regions. But the approaches on how to manipulate the chromatin state and efficiently target those genes in heterochromatin sites are lacking. The open or closed state of chromatin structure is mainly controlled by the balance of histone acetylation and deacetylation which is strictly regulated by two groups of enzymes called HAT (histone acetyltransferase) and HDAC (histone deacetylase) (22,23). Briefly, histone acetylation leads to a loose or uncoiling of the chromatin structure (euchromatin). Conversely, histone deacetylation leads to a condensed or closed chromatin structure (heterochromatin). The euchromatin gives the transcriptional machinery access to the transcriptionally active DNA (23), which also provides a great opportunity for CRISPR/Cas9 attacking and cutting the DNA, particularly for the targets located in condensed heterochromatin regions. More importantly, the chromatin state regulated by HAT and HDAC may also have the potential to influence the gene knock-in mediated by HDR (homologous directed repair), which has extremely low efficiency and needs to be improved (7,24). In addition, previous studies showed that the dCas9 (dead Cas9) fused to core p300 or HDAC3 robustly influences epigenome editing (25,26), but the effects of these HATs or HDACs on genome editing of CRISPR/Cas9 have yet to be characterized.

Given the development of histone modifiers such as HAT, HDAC inhibitors and other biotechnology approaches (27), it is possible and rational to explore whether the gene editing efficiency can be improved by altering the chromatin state through modulation of the HDAC and HAT activity. We hypothesized that the regulation of chromatin compaction by inhibiting HAT and/or HDAC activity can modulate CRISPR/Cas9 based gene editing. Our findings show that inhibition of HDAC1, HDAC2, rather than other HDACs, can enhance both gene knockout and gene knock-in. We also show that inhibition of HDAC3 could decrease the efficiency of CRISPR/Cas9 mediated gene editing. Furthermore, we provide a practical and clinically applicable approach for precise control of CRISPR/Cas9 mediated gene editing by modulation of HDAC and HAT activity in host cells.

MATERIALS AND METHODS

Cell lines

HEK293T, HeLa and HT29 cells were purchased from American Type Culture Collection (ATCC, Wesel, Germany). H27 (28), HEK.EGFP$^{TetO.KRAB}$ and HT29- EGFP is a single cell-derived clone from HeLa, HEK293 and HT29 for constitutively expressing EGFP, which have been described elsewhere (18,29,30). All cells were cultured in DMEM medium (Gibco® by Life Technologies) supplemented with 10% fetal bovine serum (FBS; Invitrogen, Breda, The Netherlands) and 1% Penicillin/Streptomycin (Gibco® by Life Technologies) at 37°C with 5% CO_2, unless otherwise indicated.

Chemical reagents

The HDAC and HAT inhibitors Entinostat, RGFP966, C646, MG149, TMP195, PC134051 were purchased from Selleckchem. The purity of these inhibitors was assessed by Selleckchem (>99%). The Entinostat analogues have been described elsewhere (31).

Cell viability detection

An MTS assay was performed to determine the dose of the HDAC and HAT inhibitors that can be administrated to the cells without affecting cell viability. Cells (3×10^3 per well) were cultured overnight and incubated with corresponding compounds in 96-well plates for 24 h. The next day, cells were incubated at 37°C with MTS for 90 min following the instruction of CellTiter 96 AQueous One Solution Reagent (Promega, Madison, USA). The absorbance was measured at the wavelength of 490 nm by a Synergy H1 plate reader (BioTek, Winooski, USA). Experiments were performed in triplicate and repeated at least three times.

Recombinant plasmids

The construction of recombinant AdV (Adenovirus) shuttle plasmids has been detailed elsewhere (32). Briefly, the recombinant plasmids contain PGK gene promoter (phosphoglycerate kinase 1) and the SV40 (simian virus 40) polyadenylation signal. The pAdSh.PGK.Cas9 has a PGK and SV40 element for controlling the hCas9 expression. The Cas9 ORF was isolated from plasmid Addgene #41815 (7). The gRNA expression units (gRNA-GFP) based on the U6 RNA Pol III promoter were retrieved from plasmids Addgene #41820 (7). The constructs above were inserted into the MCS of pAdSh.MCS.SV40, resulting in the construct pAdSh.U6.gRNA^{GFP}. The E1- and E2A-deleted fiber-modified AdV molecular clones pAdV$^{\Delta 2}$P.Cas9.F^{50} and pAdV$^{\Delta 2}$U6.gRNA^{GFP}.F^{50} were assembled in BJ5183$^{pAdEasy\text{-}2.50}$ *Escherichia coli* via homologous recombination after transformation with MssI-treated AdV shuttle plasmids (33).

For gene knock-in (EGFP-EBFP converting) experiments, the recombinant DNA has been detailed elsewhere (29). Briefly, the gRNA expression plasmid AX03_pgEGFP and the hCas9 nuclease plasmid (Addgene plasmid 41815) were used for generating DSBs at the EGFP sequence. The AX63_pTHG was used as a donor template for converting EGFP into EBFP via HDR. The AM51_pgNT was served as a negative control.

Plasmid transfection

The plasmids transient transfection using PEI (polyethyleneimine; Polysciences) has been detailed elsewhere (18).

pAdV$^{\Delta 2}$P.Cas9.F^{50} and pAdV$^{\Delta 2}$U6.gRNA^{GFP}.F^{50} viral vector production, purification and titration

The production of viral vectors AdV-Cas9 (adenovirus contains Cas9 gene) and AdV-gRNA (Adenovirus contains gRNA of eGFP sequence) are generated from

pAdV$^{\Delta 2}$P.Cas9.F^{50} and pAdV$^{\Delta 2}$U6.gRNA^{GFP}, respectively, which have been described elsewhere (32–34). Briefly, AdV particles were initiated by transfecting PER.E2A cells using PEI solution and PacI-linearized plasmids pAdV$^{\Delta 2}$P.Cas9.F^{50} and pAdV$^{\Delta 2}$U6.gRNA^{GFP}.F^{50}. After overnight incubation at 39°C, the culture media was replaced and cells were transferred to 34°C. The cells were harvested and following by three cycles of freezing and thawing in liquid nitrogen and in a 37°C water bath. Rescued AdVs presented in supernatants and amplified through propagation on PER.E2A cells newly seeded in a T75 flask. Large scale AdV produced in 16 T175 cell cultures flasks (Greiner Bio-One), following by CsCl gradient centrifugation method for purification. The titers of purified AdV were determined by TCID50 assay which has been detailed (32).

AdTL Viral vector production and purification

AdTL (Adenoviral vector) is a both E1- and E3-deleted recombinant serotype 5 adenovirus which contains a GFP (green fluorescent protein) and luciferase expression cassette (35). The HEK293 cells were seeded in 10 T175 flasks and transduced with AdTL in a dosage of 10 transduction units (TU)/cell to produce a large batch of viruses. When CPE (cytopathic effect) of 100% was reached, the cells were harvested and centrifuged at 1000 rpm for 5 min. The pellet was subjected to three cycles of freezing and thawing using dry ice and a 37°C water bath, respectively. Subsequently, the suspension was centrifuged again at 4000 rpm for 10 min. The supernatant was purified using a Q-sepharose-XL column for chromatography of adenovirus as described previously (36). Separations were carried out using a flow rate of 2 ml/min. The column was equilibrated using 25 ml application buffer (50 mM Tris–HCl pH 8,0 1.0 mM $MgCl_2$). Thereafter, the AdTL virus, dissolved in 5 ml application buffer, was loaded on the column. The column was washed with 25 ml application buffer followed by 25 ml wash buffer (containing 0.3 M NaCl). The virus was eluted from the column using 5 ml elution buffer (containing 1 M NaCl). The column was cleaned using 10 ml 0.1 M NaOH followed by 25 ml demi H_2O. An OD260 measurement was performed using the NanoDrop 1000 Spectrophotometer (ThermoFisher Scientific, USA) to determine the number of virus particles. In addition, a limiting dilution assay with AdTL dilutions was performed to determine the TCID50. Furthermore, purification by the Q sepharose XL column was checked by loading non-purified and purified AdTL virus, mixed with SDS loading buffer (4×) on a 12,5% SDS-PAGE gel, which was run for 2 h at 160 V. Subsequently, the gel was stained with Instant Blue for 30 min to make proteins visible. Furthermore, the purified virus was placed in a dialysis frame (Pierce) and dialyzed in dialysis buffer (10% glycerol, 10 mM HEPES, 1 mM MgCl, pH 7.4) to remove the elution buffer, after which a final limiting dilution assay was performed.

Transduction experiments

Cells were co-transduced with AdV-Cas9 and AdV-gRNA to measure whether HDAC/HAT inhibitors affect the quantity of EGFP gene knockout induced by CRISPR/Cas9. Cells were seeded with a density of 200 000 cells/well in a six-well plate. After 24 h, the medium was replaced by medium (5% FBS) containing HDAC/HAT inhibitors with indicated dose. After 24 h, the cells were co-transduced with AdV-Cas9 and AdV-gRNA in a quantity of 30 TU/well. All co-transductions were performed in a 1:1 ratio. Cells were subcultured for 12 days to remove EGFP protein from cells with disrupted EGFP ORFs. Subsequently, fluorescence microscopy, flow cytometry, western blot and the T7E1 assay were performed to assess which percentage of EGFP genes in cells had been cleaved by CRISPR/Cas9.

Furthermore, mock transduced H27 cells served as a control to determine the effect of the different compounds on the endogenous EGFP gene expression. Twenty four hours prior to treatment, H27 cells were seeded with a density of 200 000 cells/well. Subsequently, the cells were exposed to a medium containing the same concentrations of HDAC/HAT inhibitors as the knockout assay. After three days, flow cytometry was performed to determine the intensity of EGFP expression.

HeLa and HT29 (without EGFP) cells were transduced with the AdTL virus, which encodes for GFP and luciferase, to determine the effect of the HDAC/HAT inhibitors on transgene expression levels. HeLa cells were seeded at a density of 400 000 cells/well in a six-well plate. After 24 h, the medium was replaced by a medium containing indicated doses of HDAC/HAT inhibitors. After 24 h incubation with the compounds, AdTL was added at a dosage of 30 TU/cell. Mock- transduced cells served as control. After three days, flow cytometry was performed on the AdTL transduced cells. When a difference in transgene expression was detected, an additional experiment was performed to clarify whether the effect was due to a difference in viral transduction or transcription of the transgene. This was determined by administration of the compound 24 h prior to AdTL transduction or immediately after AdTL transduction.

Gene-editing (NHEJ and HDR) based on EGFP -to- EGFP fluorochrome conversion using plasmid donor

HEK.EGFP$^{TetO.KRAB}$ cells were seeded at 2 × 10^5 per well of six-well plates overnight. Before DNA transfection, cells were treated with indicated compounds for 48 h. The DNA transfection was performed by adding 1 mg/ml PEI with different plasmids including Cas9, pTHG. Donor and gRNA-EGFP-containing RGNs which have been detailed elsewhere (29). The different transfection complex was replaced by regular culture medium in the presence or absence of Dox (Doxycycline, Tocris Bioscience). The cells were subcultured circa every 3 days for up to 11 days. The frequencies of EGFP-negative and EBFP-positive cells cultured in medium with Dox or without Dox were determined by flow cytometry.

Cell cycle assay

Cell cycle experiment was using PI (Propidium Iodide, Sigma P4864-10ML) combined with BrdU (Bromodeoxyuridine, Sigma B5002-250MG). Briefly, cells were

seeded at 20 000 cells/well of six-well plates. BrdU was added and incubated 30 min at 37°C after 24 h HDAC inhibitors treatment with different concentrations. Next, cells were harvested and fixed using ice-cold 70% ethanol for 30 min on ice. The genomic DNA of cells were denatured by adding 2 M HCl containing 0.5% Triton X-100 and incubated for additional 30 min at room temperature. Next, BrdU-labeled cells were neutralized by adding 0.1 M $Na_2B_4O_7{\cdot}10\ H_2O$ (pH 8.5). Diluted anti-BrdU antibody (APC anti-BrdU Antibody, Biolegend) was added and incubated with cells at 4°C overnight according to manufacturer's protocol. Antibody treated cells were resuspended in 1× PBS (Phosphate Buffered Saline) contains PI (1 mg/ml) and RNase (10 mg/ml) next day. The different phases of cell cycle were determined by flow cytometry.

HDAC1, 2 and 3 knockdown by siRNAs

For HDAC knockdown, H27 and HT29 cells were transfected using Lipofectamine 2000 (Invitrogen, Carlsbad, USA). Cells were seeded at 2×10^5 per well of six-well plates overnight. On the next day, cells were transfected with siRNAs (100 nM/well) against HDAC1 (MISSION, esiRNA HDAC1), HDAC2 (MISSION, esiRNA HDAC2) and HDAC3 (M-003496-02-0005, siGENOME). siRNAs for HDAC1 and HDAC2 were purchased from Millipore Sigma (Burlington, MA, USA). siRNAs for HDAC3 were purchased from GE Healthcare Dharmacon (Lafayette, CO, USA), or control siRNAs (Burlington, MA, USA). At least three gene-specific siRNAs were used for each gene silencing. After 3 days post-transfection, cells were lysed using RIPA buffer.

RNA extraction and qRT-PCR (quantitative reverse transcriptase PCR)

Cells were washed with PBS and harvested by trypsin. RNA was extracted by the Maxwell LEV simply RNA Cells Kit (Promega, Madison, USA). RNA concentrations were determined by NanoDrop 1000 Spectrophotometer (Thermo Fisher Scientific, Waltham, USA). cDNA was synthesized using 200 ng total RNA by the Reverse Transcription kit (Promega, Madison, USA) according to the instruction. Primers are listed in Supplementary Table S1. Primers used for Cas9 and gRNA expression have been described (37). Data analysis was processed by SDS v.2.3 software (Applied Biosystems, Foster City, USA).

Fluorescence microscopy

Targeted EGFP knockout and AdTL transgene expression were monitored by fluorescence microscopy using a Zeiss Axiovert 25 CFL inverted light microscope (Carl Zeiss AG, Germany) with a 450–490 nm excitation and 515 nm emission filter set.

Flow cytometric analysis

Cells were harvested and washed twice with standard FACS buffer (PBS plus 1% FBS). The proportion of EGFP positive cells were quantified using FACS Calibur flow cytometer (BD, Franklin Lakes, USA). For EGFP and EBFP converting mediated gene knock-in study, the BD FACSVerse cytometer (BD, Franklin Lakes, USA) was used. All the experiments were performed at the Central Flow cytometry Unit (University Medical Center Groningen). Data were analysed by FlowJo 7.2.2 software (Tree Star).

Immunoblotting

Cells were washed with PBS and harvested by trypsinization. Cells were lysed using RIPA buffer with PIC (Protease Inhibitor Cocktail; Thermo Fisher Scientific, USA). Protein concentrations were determined by a Pierce BCA Protein Assay Kit (Thermo Fisher Scientific, USA). Samples were separated by pre-cast SDS-PAGE (Bio-Rad, Hercules, USA) and transferred using a PVDF membrane (polyvinylidene difluoride). The PVDF membrane was blocked with 5% skimmed milk in PBST (0.1% Tween-20) at room temperature for 1 h and incubated at 4°C overnight with primary antibodies. Anti-rabbit or anti-mouse HRP conjugated antibodies were used to detect protein by chemiluminescence using ECL (Perkin Elmer, Western Lightning Plus ECL). Images were visualized by GeneSnap image analysis software (SynGene, Frederick, USA) and quantified with ImageJ software (National Institute of Health, USA). The following antibodies from Cell Signalling were used for immunoblotting, Cas9 (#14697), HDAC1 (#2062), HDAC2 (#5113) and HDAC3 (#2632). The dilution of primary antibodies was 1:1000 (v/v). The secondary antibodies rabbit anti-mouse (#P0260) and goat anti-rabbit (#P0448) HRP were purchased from Dako Denmark. The dilution of secondary antibodies was 1:2000 (v/v). The dilution of fluorescent secondary antibody (#92632211 and #92668070) was 1:10000 (v/v).

Chromatin immunoprecipitation (ChIP) and qPCR

Chromatin immunoprecipitation (ChIP) and qPCR were performed to detect the alterations of chromatin state and the binding of Cas9 to targeted DNA in the presence or in the absence of HDAC inhibitors. The cells were cultured in the presence or absence of inhibitors at an indicated dose for 3 days, after which cell fixation was applied according to the protocol as described before (18). Briefly, 2 ml of 11% formaldehyde solution were added to the cell culture medium. The culture flasks were agitated for 15 min at room temperature. Next, 1.1 ml of 2.5 M glycine was used to stop the fixation process. After a 5 min incubation at room temperature, cells were transferred to a 50 ml tube. The harvested cells were subjected to centrifugation at 1350 × g for 5 min at 4°C for two cycles with PBS. Subsequently, the nuclei were isolated using pre-chilled solution (0.1% NP-40 in PBS) and collected by centrifuging at 10 000 rpm at 4°C for 10 s. Next, to obtain DNA fragments, MNase (Micrococcal Nuclease) was used according to the manufacturer's instruction. The ChIP-qPCR assays were carried out on 30 μg of cross-linked chromatin according to the HistonePath™ (Active Motif) ChIP-qPCR protocol. The ChIP-validated antibodies H3 pan-acetyl (Active Motif, cat # 39139) and Cas9 antibody (mAb) (8C1-F10) were used for the ChIP. Next, qPCR amplifications with primers targeting different regions (i.e. EF1α promoter, 5′ and 3′ EGFP gene segments) were performed. For Cas9 ChIP-qPCR, EGFP

ORF primers were used. Additional primer pairs were used for the quality control of the ChIP-qPCR assays. All of the primer sequences have been detailed (18).

The qPCR amplifications were performed in an ABI Prism 7900HT Sequence Detection System. The qPCR amplifications were performed in triplicate for each sample with the following procedures: a 2-min incubation period at 95°C, followed by 40 cycles with at 95°C for 15 s, at 58°C for 20 s at 72°C for 20 s. Next, the samples were incubated at 95°C, 55°C for 1 min, respectively. The binding events detecting every 1000 cells were calculated based on input amounts of chromatin, final ChIP volumes, and the primer efficiencies. Finally, the data were normalized according to the algorithm developed by Active Motif, Inc. (Carlsbad, CA, USA), which is available as an online tool (https://www.activemotif.com).

MNAse-qPCR

MNAse-qPCR protocol was adapted from an earlier described method (38). In brief, nuclei were isolated by resuspending a cell pellet in 1 ml of ice-cold PBS containing 0.1% NP-40 supplemented with 1× PIC (cOmplete™, Mini, EDTA-free, Roche). The cell suspension was vortexed for five seconds at max. speed followed by centrifugation for 5–10 s at 9000 × g. The supernatant was discarded and the pellet was resuspended in 1 ml ice-cold PBS containing 0.1% NP-40 supplemented with 1× PIC to wash the nuclei. The nuclei were spun down again for 5–10 s at 10 000 rpm and the supernatant was again discarded. Next, the nuclei were resuspended in 100 μl MNAse buffer (50 mM Tris–HCl, 5 mM $CaCl_2$, 100 μg/ml BSA, pH 7.9) and warmed to 37°C in a water bath, followed by addition of 5 U (unit) MNAse (NEB, diluted to 1 U/μl in MNAse buffer). MNase digestion was stopped after 5 min by adding EDTA to a final concentration of 5 mM and cooling on ice. The suspension was spun down for 5–10 s at 10 000 rpm and the supernatant was transferred to a new tube (pellet contains nuclear debris). Proteinase K was added to a final concentration of 1 mg/ml and incubated for 1 h at 50°C. DNA was size selected and purified with Ampure beads according to the manufacture's protocol (AMPure XP, A63881, Beckman Coulter, USA). First 0.7× sample vol. of Ampure beads were added and after a 5 min incubation at room temperature the beads were discarded (to discard large DNA fragments). Next, 1.8× original sample vol. Ampure beads were added and work-up was performed according to the product manual. The DNA was eluted in 80 μl water.

The qPCR amplifications were performed in an ABI Prism 7900HT Sequence Detection System. The protocol was described as previously. Data were analyzed using QuantStudio™ Real-Time PCR software (ThermoFisher Scientific, USA).

T7E1 assay

To determine the genome targeting efficiency of CRISPR/Cas9, T7E1 (T7 endonuclease 1 assay) was performed. H27 cells were harvested and genomic DNA was isolated using Genomic DNA purification kit (Qiagen, Germany) following the manufacturer's instructions. The concentration of the isolated genomic DNA was determined using The NanoDrop 1000 Spectrophotometer (ThermoFisher Scientific, USA). Thereafter, a PCR was performed using Taq polymerase (NEB, USA) with primers 5′ GAGCTGGACGGCGACGTAAACG 3′ and 5′ CGCTTCTCGTTGGGGTCTTTGCT 3′ for amplification (Sigma-Aldrich, Germany). The PCR amplification was as follows: an initial denaturation 95°C for 5 min, samples were subjected to 35 cycles of denaturation at 95°C for 30 se, annealing at 53°C for 30 s and elongation at 72°C for 40 s. Amplified DNA products were mixed with 1.5 μl NEB Buffer 2 and 3.0 μl nuclease-free water. An initial denaturation was performed following a ramp rate −2°C /second from 95°C and then −0.1°C /second from 85°C to 25°C. Subsequently, 1 μl T7E1 enzyme (NEB, USA) was added and incubated at 37°C in a water bath for 15 min. Gel electrophoresis was performed for detecting DNA fragments.

Sanger sequencing for detection of off-target effects

Sanger sequencing was performed by Eurofins Genomics' DNA sequencing service according to the instruction. The primers are listed in supplementary data.

Nextera XT DNA Library Prep for Next-Generation Sequencing

Input DNA was tagmented and amplified using Illumina's Nextera XT DNA Library Prep. Libraries were quantified with Thermo's Qubit high-sensitivity DNA kit and run on the Agilent high sensitivity D1000 ScreenTape system for quality control. Sequencing was performed on NextSeq 500 (Illumina) using NextSeq 500 75-cycle High Output kit v2.5.

Bioinformatic analysis

Reads were aligned using bowtie2 v2.2.4. against 710 bp reference sequence. Indel realignment was performed using GATK version 3.8.0 on merged (all libraries analysed) BAM files. Quantification of polymorphisms was done with help of samtools mpileup command. A custom Perl script (available upon request) was used to parse the output into a summary table.

Statistical analysis

The data were presented as mean ± SD (unless otherwise indicated). Data were derived from at least three independent experiments (unless otherwise indicated). Statistical analysis was performed by GraphPad software v.5.0 (La Jolla, CA, USA). Data were analyzed by a two-tailed unpaired Student's *t*-test (unless otherwise indicated). **P*-values < 0.05; ***P*-values < 0.01; ****P*-values < 0.001.

RESULTS

The landscape of HDAC/HAT inhibition on CRISPR/Cas9-mediated gene knockout

To investigate the effect of different HDACs/HATs on

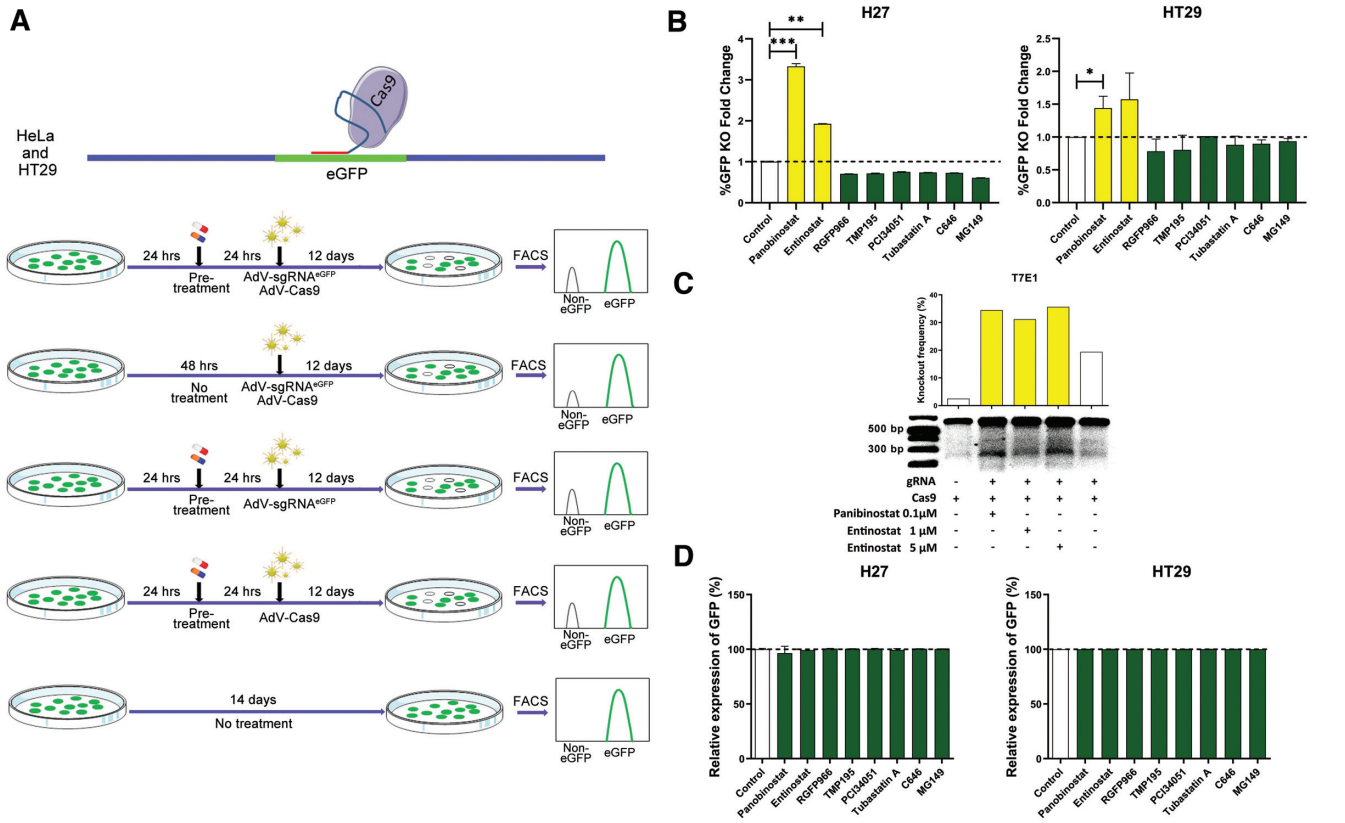

Figure 1. Screening HDAC inhibitors for improving CRISPR/Cas9 mediated gene editing. (**A**) Schematics of HDAC inhibitors screening procedures for CRISPR/Cas9 mediated gene knockout. CRISPR/Cas9 specifically cuts the EGFP sequence in HeLa (H27) and HT29 cells resulting in EGFP signal loss (28,30,32). Cells were pre-treated with different inhibitors and incubated with AdV-Cas9 and AdV-gRNA, subsequently subcultured for 12 days to remove EGFP protein from cells with disrupted EGFP ORFs. EGFP Gene editing efficiency is measured by FACS. (**B**) The effect of different HAT/HDAC inhibitors on CRISPR/Cas9 mediated gene knockout in H27 and HT29 with Panobinostat (0.1 μM), Entinostat (5 μM), RGFP966 (1 μM), TMP195 (1 μM), PCI34051 (1 μM), Tubastatin A (1 μM), C646 (1 μM) and MG149 (1 μM). The frequencies of gene knockout were quantified by flow cytometry. (**C**) T7EI genotyping assays for detection of indels induced by CRISPR/Cas9 in H27 cell line and quantified by ImageJ. (**D**) Endogenous EGFP expression determined by flow cytometry with the treatment of different HDAC/HAT inhibitors. Data in bar graphs are represented as mean ± SD ($n \geq 3$), two-tailed unpaired Student's *t*-test: **P*-values < 0.05; ***P*-values < 0.01; ****P*-values < 0.001.

CRISPR/Cas9-mediated gene knockout, we tested a panel of HDAC/HAT inhibitors (Table 1) with a CRISPR/Cas9-mediated EGFP (enhanced green fluorescent protein) knockout reporter system (32) (Figure 1A). H27 and HT29-EGFP is a single cell-derived clone from HeLa and HT29 for constitutively expressing EGFP, which have been described elsewhere (18,28–30).

To preclude the interference of drug toxicity, we performed a cell viability assay with the treatment of HDAC/HAT inhibitors in H27 and HT29 cells (Supplementary Figure S1). At least 90% of cell viability compared to the control group was considered as acceptable. According to the cell viability data (Supplementary Figure S1), the dose of each inhibitor without affecting cell viability are Panobinostat (0.1 μM), Entinostat (5 μM), RGFP966 (1 μM), TMP195 (1 μM), PCI34051 (1 μM), Tubastatin A (1 μM), C646 (1 μM) and MG149 (1 μM) (Supplementary Figure S1A).

A co-transduction grid experiment was performed to assess which dosage of virally delivered gRNA and Cas9 results in high genomic EGFP gene knockout levels without reducing cell viability. We observed that a dosage of 30 TU/cell resulted in relatively high amounts of EGFP gene knockout as well as no reduction of cell viability (Supplementary Figure S2). Therefore, we transduced 1:1 mixtures of and gRNA and Cas9 viral particles at 30 TU/cell, respectively, to induce DSBs at EGFP sequences. The EGFP gene editing frequencies were determined by direct fluorescence microscopy and flow cytometry at 14 days post-transduction. Our results showed that Entinostat (HDAC1/2/3 inhibitor) and Panobinostat (pan-HDAC-inhibitor) significantly increased gene knockout frequencies in both H27 and HT29 cells by 1.5–3.4-fold (Figure 1B). Of note, RGFP966 (HDAC3 inhibitor) slightly decreased gene knockout frequencies as well as other HDAC inhibitors (HDAC4–9) (Figure 1B). Additionally, HAT inhibitors C646 (p300/CBP inhibitor) and MG149 (Tip60 and MOZ inhibitor) decreased the EGFP gene knockout frequencies (Figure 1B). The gene knockout frequencies enhanced by Entinostat and Panobinostat were further determined by T7E1 (T7 endonuclease I) assay (Figure 1C). As controls, we did not observe gene knockout in the groups with a single treatment (gRNA only, Cas9 only, inhibitors only) and non-treatment groups. To evalu-

Table 1. List of HDAC/HAT inhibitors used in this study

Name	HDAC1	HDAC2	HDAC3	HDAC4	HDAC5	HDAC6	HDAC7	HDAC8	HDAC9	P300/CBP	Tip60 and MOZ
Panobinostat	+	+	+	+	+	+	+	+	+	–	–
Entinostat	+	+	+	–	–	–	–	–	–	–	–
RGFP966	–	–	+	–	–	–	–	–	–	–	–
TMP195	–	–	–	+	+	–	+	–	+	–	–
Tubastatin A	–	–	–	–	–	+	–	–	–	–	–
PCI34051	–	–	–	–	–	–	–	+	–	–	–
C646	–	–	–	–	–	–	–	–	–	+	–
MG149	–	–	–	–	–	–	–	–	–	–	+

ate CRISPR/Cas9 target efficiency more precisely, we have performed next generation sequencing to measure the targeting efficiency. We observed a significant increase of target efficiency using Entinostat and Panobinostat. According to the next generation sequencing data, Entinostat and Panobinostat increase the gene editing frequency by 3.7-fold and 10.5-fold, respectively (Supplementary Figure S3).

To assess the possibility of the impacts of HDAC inhibitors on endogenous EGFP expression in H27 and HT29, we tested the EGFP expression level using flow cytometry and there were no changes of endogenous EGFP expression, indicating no affection on endogenous EGFP expression upon these HAT/HDAC inhibitors treatments (Figure 1D).

Panobinostat and Entinostat enhance CRISPR/Cas9-mediated gene knockout in a dose-dependent manner.

Next, we asked whether the enhancement of gene knockout by Panobinostat and Entinostat is dose dependent. We tested the indicated amounts of Panobinostat and Entinostat (Figure 2). Our results showed a positive correlation between the EGFP gene knockout frequencies and the dose of Panobinostat and Entinostat (Figure 2). These results clearly indicate that Panobinostat and Entinostat enhance CRISPR/Cas9-mediated gene knockout in a dose-dependent manner.

Downregulation of HDAC1 or HDAC2 increases gene knockout efficiency

Both Panobinostat (a pan-HDAC inhibitor) and Entinostat (an HDAC1/2/3 selective inhibitor) enhanced gene knockout, but RGFP966 (an HDAC3 selective inhibitor) decreased gene knockout. Moreover, we did not observe the enhancement of gene knockout by other HDAC selective inhibitors. Therefore, we speculate that HDAC1/2/3 may play an important role in the gene editing process of CRISPR/Cas9. To precisely distinguish the role of the three HDACs in gene editing processes, we used siRNAs to specifically knockdown HDAC1, HDAC2 or HDAC3 to explore whether gene knockout efficiency can be enhanced or decreased (Figure 3A). In agreement with the inhibitors results above, we showed that knockdown of HDAC1 or HDAC2 results in a significant increase by 16–28% and 22–26% ($P < 0.01$) of EGFP gene knockout, respectively (Figure 3B). Moreover, our results showed that downregulation of HDAC3 decreased the EGFP gene knockout efficiency by 21% and 39% ($P < 0.001$) in H27 and HT29 cell lines, respectively (Figure 3B). Thus, downregulation of HDAC1 or HDAC2 increases CRISPR/Cas9-mediated gene knockout, but downregulation of HDAC3 decreases it.

Effect of Panobinostat and Entinostat on viral transduction, transgene transcription and cell cycle

Although we hypothesized that HDAC inhibitors may increase the CRISPR/Cas9 mediated gene editing by increasing the accessibility of the target loci, viral transduction and transgene transcription might also influence the gene knockout, particularly by affecting Cas9 protein expression levels. Therefore, additional experiments were performed to determine the influence of Panobinostat and Entinostat on viral transduction and transgene expression.

To explore the impacts of Panobinostat and Entinostat on adenovirus transduction and transgene expression, we first tested with an EGFP reporter AdTL (Adenoviral vector). Since H27 and EGFP-HT29 cells have endogenous EGFP expression which may affect the measurement, the original HeLa and HT29 cells without EGFP expression were employed. HeLa and HT29 wild-type cells were treated with Entinostat and Panobinostat, respectively, prior and post to AdTL infection to determine adenovirus transduction and transgene expression. Subsequently, the effect of these HAT/HDAC inhibitors on the expression of GFP was evaluated by flow cytometry. The results showed that the expression of exogenous GFP by AdTL increased dramatically upon Panobinostat treatment in both pre- and post-treatment (Figure 4A). In contrast, in the cells treated with Entinostat there was no significant change (Figure 4A). These results indicate that Entinostat does not affect adenovirus transduction and transgene expression.

To directly determine the effects of Panobinostat and Entinostat on Cas9 expression, H27 and HT29 cells were treated with Entinostat and Panobinostat, prior to AdV-Cas9 infection. Subsequently, the effects of these HAT/HDAC inhibitors on RNA levels of Cas9 and gRNA were measured by qPCR and Cas9 protein levels were determined by Western blot. We observed that Panobinostat significantly increased RNA levels of Cas9 as well as protein expression in HT29 cells, but Entinostat did not show a significant increase of Cas9 expression in both RNA and protein levels (Figure 4B and C). Interestingly, we observed Entinostat decreases gRNA expression levels in both cell lines. Panobinostat increases gRNA expression in H27, but decreases in HT29 (Figure 4B). These data indicated that the increase of gene knockout by Panobinostat may be

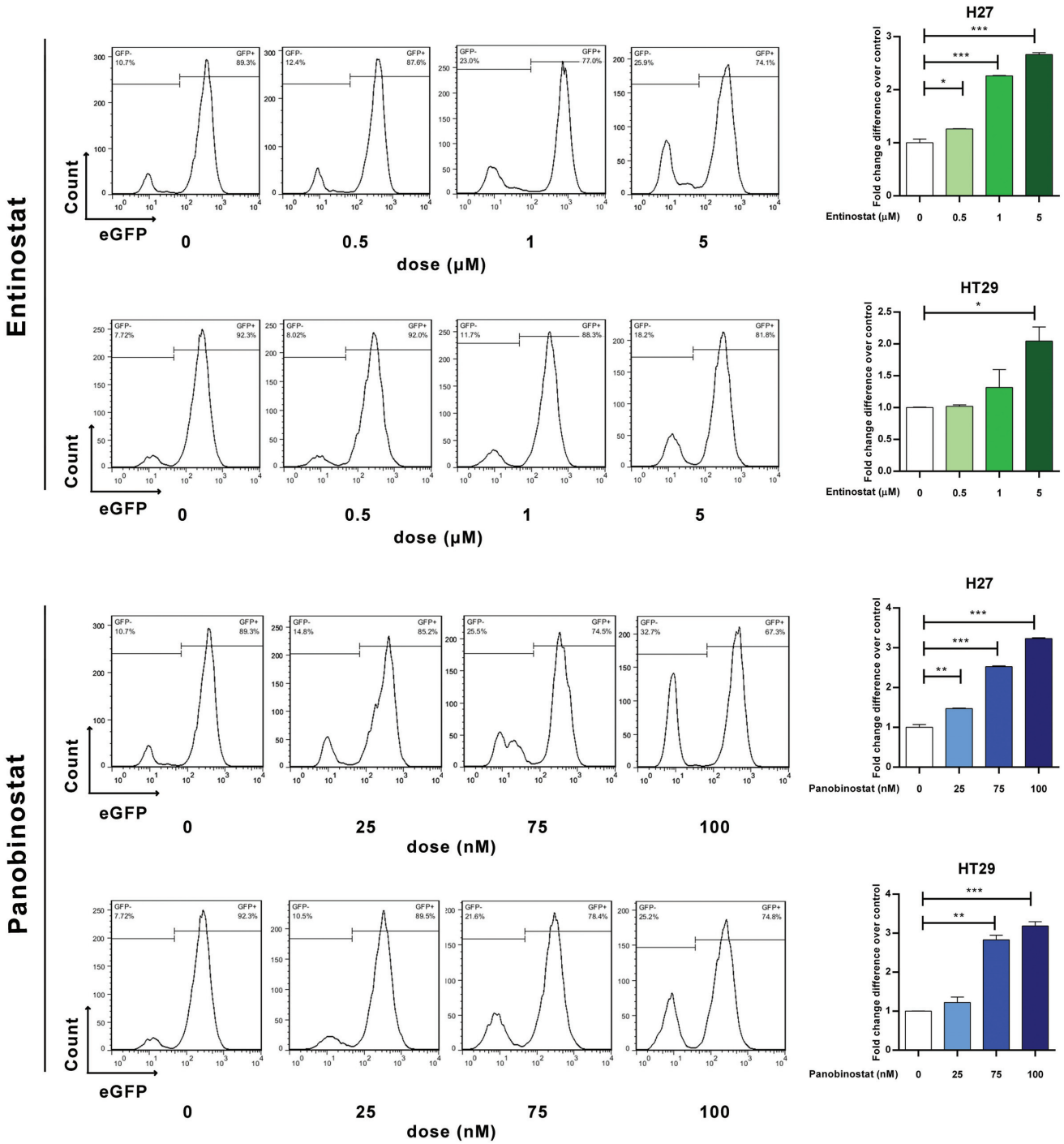

Figure 2. Dose dependent effects of Entinostat and Panobinostat on CRISPR/Cas9 mediated gene knockout. The dosage of Entinostat are 0, 0.5, 1 and 5 μM and Panobinostat are 0, 25, 75, 100 nM. Dose-dependent response to Entinostat and Panobinostat was assessed by flow cytometry. Data were derived from three independent experiments. The quantification bar graph (right) generated according to flow cytometry data (left). Data in bar graphs are represented as mean ± SD ($n \geq 3$), two-tailed unpaired Student's *t*-test: **P*-values < 0.05; ***P*-values < 0.01; ****P*-values < 0.001.

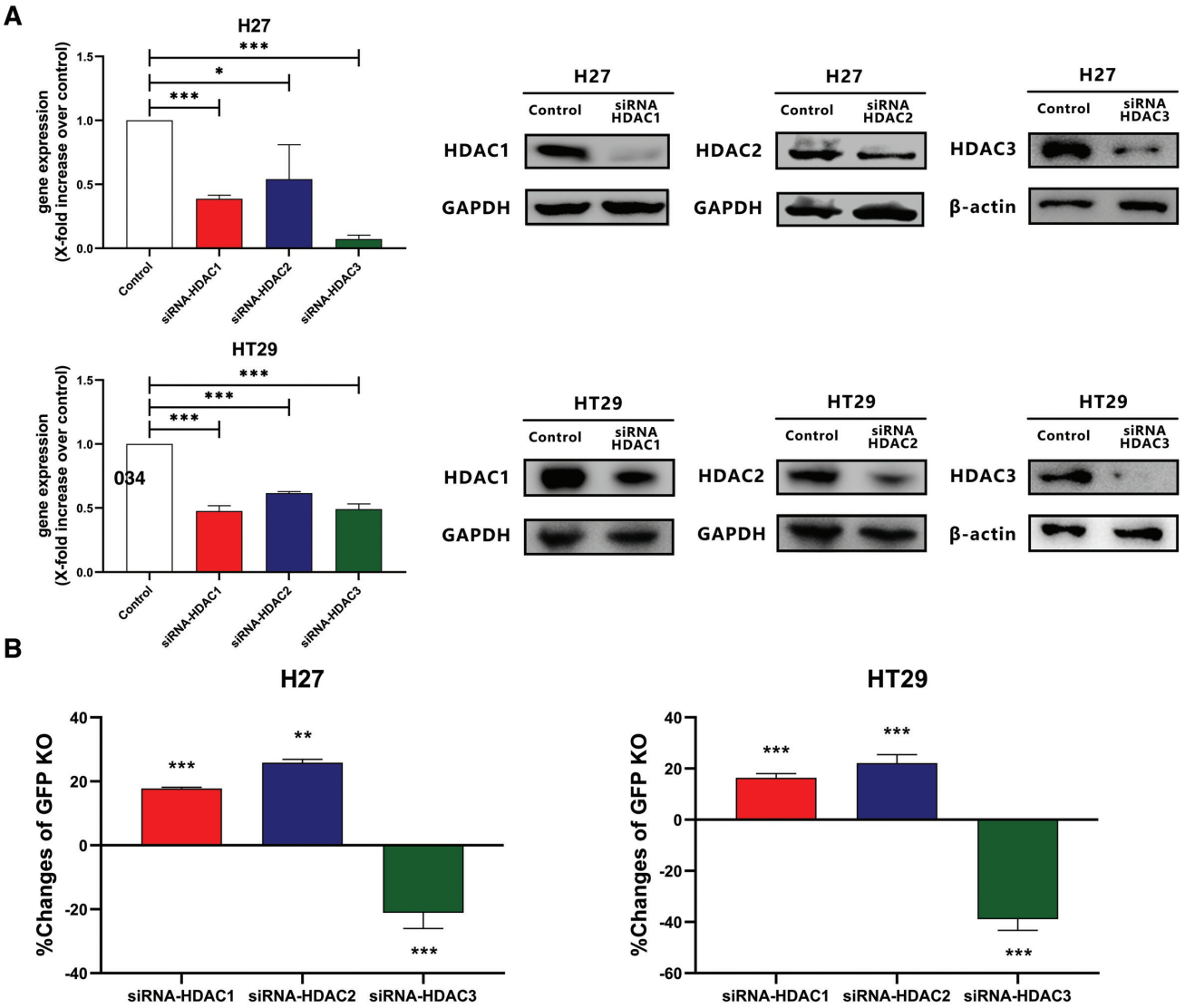

Figure 3. Assessment of gene knockout frequencies by knockdown of HDAC1, HDAC2 and HDAC3. (**A**) HDAC1, HDAC2 and HDAC3 mRNA and protein levels were determined by RT-qPCR and western blot after transfection with scrambled siRNAs or HDAC1, HDAC2 or HDAC3 siRNAs. (**B**) Changes of EGFP knockout mediated by CRISPR/Cas9 upon knockdown of HDAC1, HDAC2 or HDAC3. Data in bar graphs are represented as mean ± SD ($n \geq 3$), two-tailed unpaired Student's *t*-test: **P*-values < 0.05; ***P*-values < 0.01; ****P*-values < 0.001.

due to Cas9 protein upregulation, but this was not the case for Entinostat. Furthermore, we checked the Cas9 expression with post-treatment. There were no obvious changes of Cas9 expression with post-treatment of Panobinostat and Entinostat (Supplementary Figure S4). These results suggest that Panobinostat may increase Cas9 expression by enhancing viral transduction, but not transgene expression.

To investigate the effects of the accessibility of the viral particles to cell membrane with Entinostat and Panobinostat treatment, we measured the expression levels of cellular receptor CD46 for adenoviruses by flow cytometry analysis (32). Our results show that only Panobinostat significantly increases CD46 expression levels in H27 cells (Supplementary Figure S6). Thus, Panobinaostat might increase virus transduction via CD46 upregulation.

DSBs introduced by CRISPR/Cas9 are repaired by either non-homologous end joining (NHEJ) or homology directed repair (HDR). However, these two repairing pathways favour a specific cell cycle. NHEJ is active throughout the cell cycle, but it has the highest activity in S and G2/M stages[17], whereas HDR is most efficient in S and extremely low in G1 (39). Therefore, HDAC and HAT inhibitors might regulate the gene editing efficiency by affecting the cell cycle. Particularly, Panobinostat has been reported to arrest cell cycle at G2/M (40). To determine the cell cycle changes introduced by Entinostat and Panobinostat, we performed flow cytometry analysis of cell cycle using PI DNA staining incorporating a proliferative marker BrdU. Panobinostat arrested cells at G2/M (0.075 μM and 0.1 μM), but we did not observe an obvious cell cycle change in the treatment of Entinostat (Figure 4D).

Collectively, these results show that Panobinostat and Entinostat enhance gene knockout by different mechanisms. The increase of Cas9 expression and G2/M cell cy-

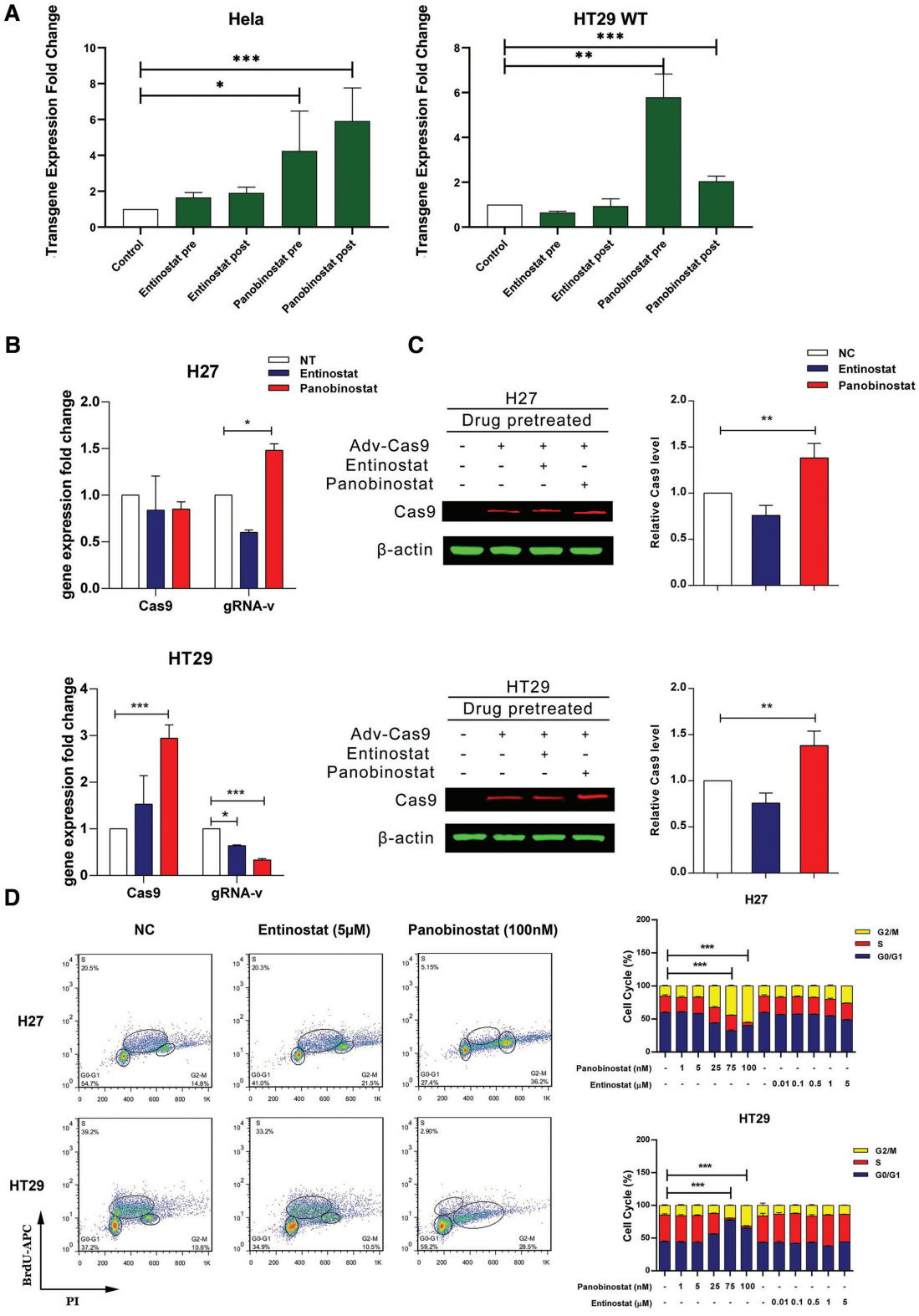

Figure 4. Alterations of virus transduction, transgene transcription and cell cycle with the treatment of Entinostat and Panobinostat. (**A**) AdTL-EGFP transgene expression was determined by flow cytometry with the pre- and post-treatment of HDAC inhibitors. (**B**) RNA level of Cas9 and gRNA expression level are measured by qPCR. (**C**) AdV-Cas9 protein expression was determined by western blot with pre-treatment of HDAC inhibitors (Entinostat 5 μM, Panobinostat 0.1 μM) and Western blot quantification. The graph was generated through quantifying blots from three independent experiments by ImageJ. (**D**) Cell cycle changes incorporate with Brdu upon HDAC inhibitors treatment with different dose. Data in bar graphs are represented as mean ± SD ($n \geq 3$), two-tailed unpaired Student's *t*-test: **P*-values < 0.05; ***P*-values < 0.01; ****P*-values < 0.001.

cle arrest may contribute to gene knockout enhancement induced by Panobinostat, which might be different to our initial hypothesis, whereas, Entinostat is consistent with our hypothesis.

Entinostat analogues significantly enhance the CRISPR/Cas9 gene knockout efficiency

Owing to the promising results of Entinostat for improving CRISPR/Cas9 gene editing efficiency, we tested three analogues of Entinostat to confirm our findings (31) (Figure 5A). These three Entinostat analogues significantly increased the gene knockout frequencies (30–52%) of CRISPR/Cas9 without effects on cell viability (Figure 5B and Supplementary Figure S1B). In consistence with Entinostat, these analogues have no effect on endogenous EGFP expression (Figure 5C), Cas9 expression (Figure 5D and Supplementary Figure S4) and cell cycle (Figure 5E). Furthermore, we did not observe significant changes of cell doubling time (41) and morphology with Entinostat treatment, but those changes have been observed with Panobinostat treatment (Supplementary Figure S8).

Panobinostat and Entinostat significantly enhance gene knock-in (HDR) and knockout (NHEJ)

The gene knock-in efficiency by HDR pathway is much lower than gene knockout by NHEJ. To investigate whether our inhibitors can enhance the gene knock-in efficiency, an EGFP-EBFP converting fluorescent system was employed (42). This system allows the simultaneous detection of mutagenic NHEJ and HDR events (Figure 6A). In parallel, the chromatin compaction can be precisely regulated by Dox (doxycycline) treatment. The heterochromatin will be formed in the targeted sequences in the absence of Dox. After the gene editing process, Dox is added to determine the frequencies of mutagenic NHEJ and HDR events through dual-color flow cytometry (Figure 6A).

Entinostat increased the mutagenic NHEJ and HDR rate by ∼2.3-fold, ∼2.4-fold, respectively (Figure 6B). Panobinostat increased the NHEJ and HDR rate by ∼2.6-fold, ∼1.4-fold, respectively (Figure 6B). However, RGFP966 decreased both knockout and knock-in. In agreement with the data from the adenovirus system, alterations of gene knockout with this plasmid transient transfection system were similar, which confirms our previous data. Meanwhile, we performed a cell viability assay to determine that the concentrations of the compounds we used have no effect on cell proliferation (Supplementary Figure S1C).

We further determined the effects of Panobinostat and Entinostat on gRNA and Cas9 expression by qRT-PCR and Western blot. We did not observe changes of Cas9 expression levels after treatment with either Panobinostat or Entinostat (Figure 6C and D). However, the expression of gRNA increased after treatment of Panobinostat (Figure 6C). These results suggest that the enhancement of gene knock-in/knockout by Entinostat is not due to gRNA and Cas9 expression changes. In addition, we also checked the Cas9 expression with Panobinostat or Entinostat post-treatment. Panobinostat slightly enhanced Cas9 protein level with post-treatment in H27, but this was not the case for Entinostat (Supplementary Figure S5). Furthermore, we checked the Cas9 expression with pre- and post-treatment of all Entinostat analogues (Figure 5A) and found that there were no increases of Cas9 expression (Supplementary Figure S5). Additionally, Panobinostat and Entinostat showed no significant effect on the cell cycle of HEK.EGFP$^{TetO.KRAB}$ (Figure 6E).

Chromatin immunoprecipitation (ChIP)-qPCR and MNase (micrococcal nuclease)-qPCR revealed Entinostat and Panobinostat introduced an open state of chromatin in the target loci

To gain insight into the chromatin state at the CRISPR/Cas9 target region, ChIP-qPCR assays were performed in the presence or absence of Entinostat (5 μM) and Panobinostat (0.1 μM) in H27 cells. A ChIP-grade antibody against H3Ac (histone3-acetylation), which commonly serves as a marker of open chromatin status, was used. With the treatment of Entinostat and Panobinostat, the enrichment for the euchromatin marker H3Ac were ∼1.7-fold and ∼2.9-fold higher than with no treatment group, respectively (Figure 7A). Therefore, the HDAC inhibitors (Entinostat and Panobinostat) induced the euchromatin state in the CRISPR/Cas9 target region.

MNase-qPCR is able to precisely determine chromatin structure and DNA accessibility at specific target loci with light-digestion conditions by concentration of MNAse (5 U) and the short time of incubation (5 min) (43). Therefore, we performed MNase-qPCR to measure how Entinostat and Panobinostat influenced chromatin structure and DNA accessibility at CRISPR/Cas9 target region. Our results show that both Entinostat and Panobinostat can significantly increase DNA accessibility around the gRNA binding site on EGFP (Figure 7B).

To further determine the binding of Cas9 protein and target loci of chromosome in a direct manner, ChIP-qPCR assays were performed using a specific Cas9 antibody as well. The enrichment of Cas9 protein binding to target DNA was ∼3.0-fold and ∼1.7-fold higher than the group with no Entinostat or Panobinostat treatment (Figure 7C). Of note, enrichment of Cas9 protein binding to targeted DNA was consistency with gene knock-in results (Figure 6B). Collectively, these results provide direct evidence for HDAC inhibitors improving the accessibility of chromatin and increasing the binding of Cas9 and targeted DNA (Figure 8).

Detection of off-target effects by Sanger sequencing

To detect whether Entinostat can increase off-target effects, we have amplified the DNA by PCR with specific primers (Supplementary Table S2) and performed Sanger sequencing to detect four potential off-target sites in genome selected from Cas-OFFinder (36). We did not observe any off-targets in these regions with/without treatment of Entinostat (5μM) (Supplementary Figure S7) in H27 cells. However, we cannot completely rule out any other remaining off-target possibilities due to the limitation of our detection methods.

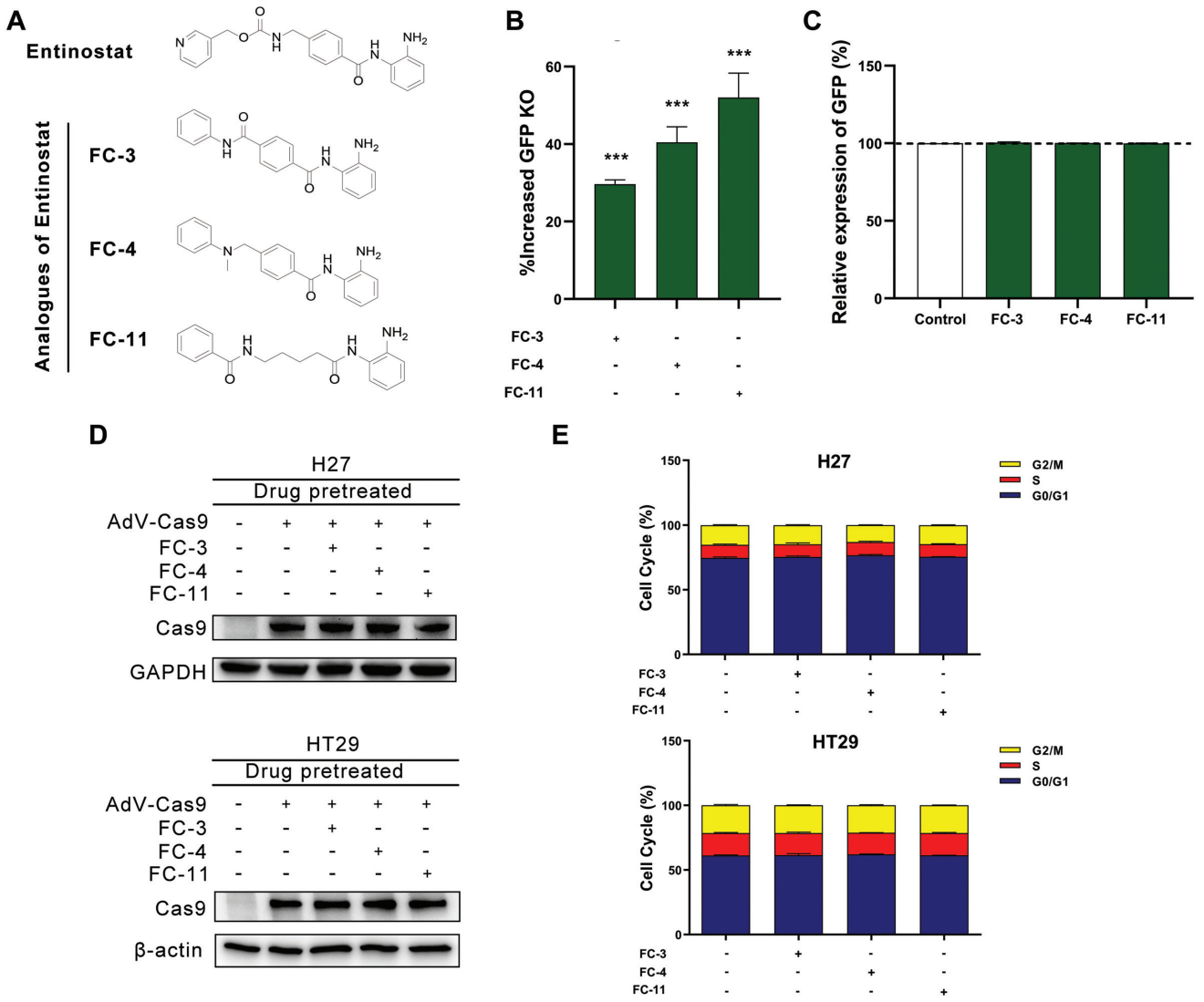

Figure 5. Entinostat analogues on CRISPR/Cas9 mediated gene editing. (**A**) The chemical structures of Entinostat and its analogues. (**B**) Gene knockout enhanced by Entinostat analogues treatment. (**C**) Endogenous EGFP expression changes by Entinostat analogues treatment. (**D**) Cas9 protein expression changes by Entinostat analogues treatment. (**E**) Cell cycle changes by Entinostat analogues treatment. The dose of analogues used are 1 μM FC-3, 1 μM FC-4, and 10 μM FC-11. Data in bar graphs are represented as mean ± SD ($n \geq 3$), two-tailed unpaired Student's *t*-test: **P*-values < 0.05; ***P*-values < 0.01; ****P*-values < 0.001.

DISCUSSION

We comprehensively investigated the impact of HDACs and HATs on CRISPR/Cas9 mediated gene editing. We found that Entinostat (HDAC1/2/3 inhibitor) and Panobinostat (pan-HDAC inhibitor) enhanced Cas9 gene editing activity while other inhibitors (HDAC4/5/6/7/8/9) did not. We also found that RGFP966 (HDAC3 inhibitor) decreased CRISPR/Cas9 gene editing activity, which can be used for downregulation CRISPR/Cas9 gene editing activity. Importantly, Entinostat and Panobinostat dramatically increase gene knock-in rates. We confirmed these findings by knockdown of HDAC1, HDAC2 and HDAC3. We further identified that HDAC inhibition (Entinostat and Panobinostat) facilitated Cas9 access to target DNA and increased cutting frequencies. Our study revealed an essential role of HDACs in CRISPR/Cas9 mediated gene editing. We demonstrate that it is feasible to modulate CRISPR/Cas9 gene editing efficiency by regulating HDAC activity. This method might also be widely used in regulating other nucleases (ZFNs, TALENs, CRISPR/Cas9 and dCas9)-mediated genome and epigenome editing.

We showed that inhibition of HDAC1 or HDAC2, but not other HDACs or HATs, significantly enhances the gene knockout and knock-in frequencies by uncoiling the chromatin structure. Several recent studies showed that the chromatin structure and nucleosomes dramatically affect CRISPR/Cas9 mediated gene editing (17,18,20,44). For instance, a study shows that nucleosomes inhibit CRISPR-Cas9 cleavage activity via blocking binding of Cas9 to PAM sites (20). Another study shows heterochromatin delays CRISPR-Cas9 mutagenesis, but does not affect the outcome of mutagenic DNA repair. They also show that mu-

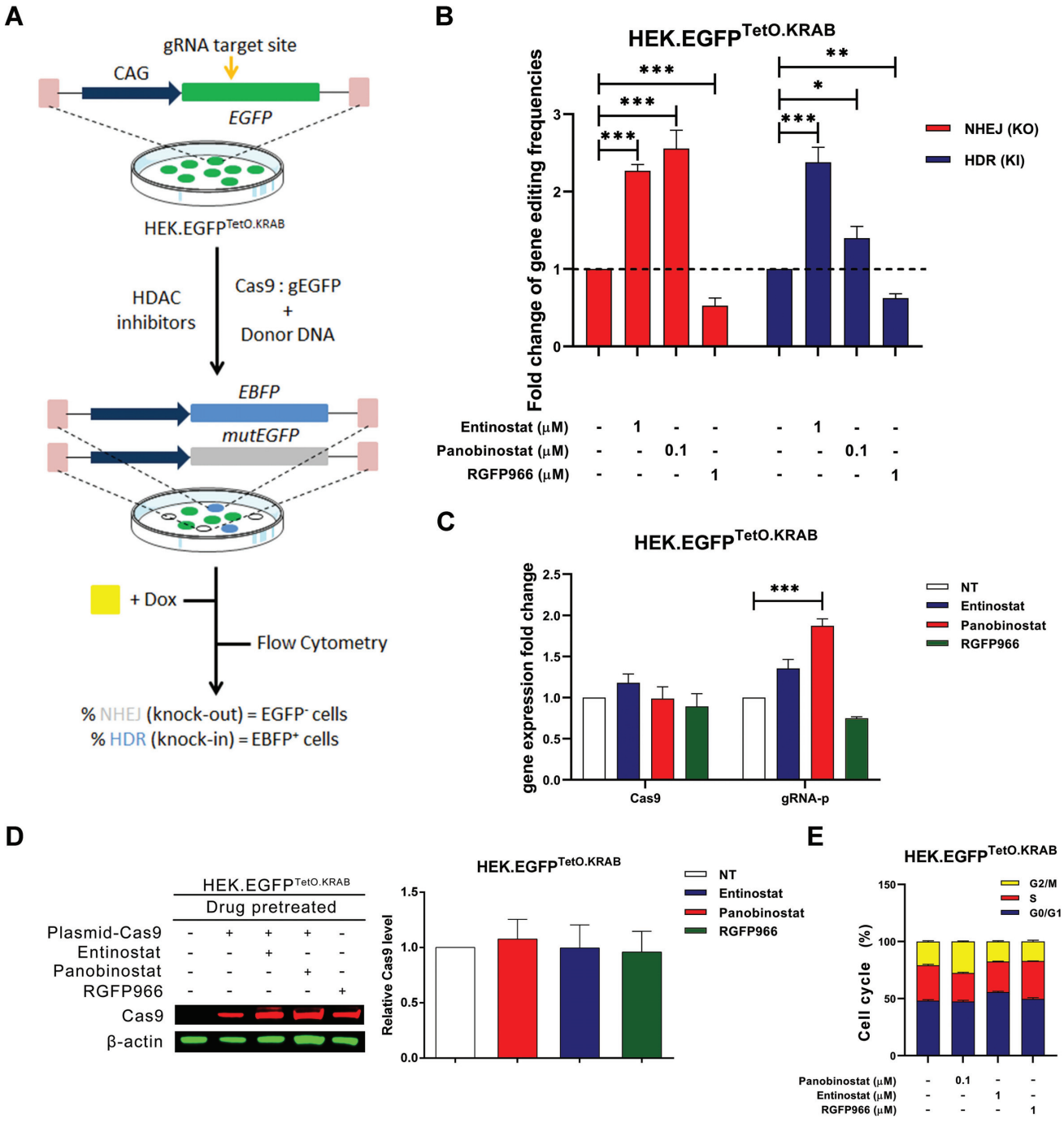

Figure 6. Gene-editing (NHEJ and HDR) based on converting EGFP to EBFP fluorochrome with a plasmids transient transfection system. (**A**) Schematic representation of a knockout and knock-in system by converting EGFP to EBFP. (**B**) Alterations of gene knockout and knock-in with different HDAC inhibitors treatment. (**C**) RNA level of Cas9 and gRNA expression level are measured by qPCR. (**D**) Cas9 protein expression changes with different HDAC inhibitors treatment using the same dose as shown in knock-in. (**E**) Cell cycle changes by Panobinostat, Entinostat, and RGFP966 treatment. The dose of HDAC inhibitors are used as shown. Data in bar graphs are represented as mean ± SD ($n \geq 3$), two-tailed unpaired Student's *t*-test: **P*-values < 0.05; ***P*-values < 0.01; ****P*-values < 0.001.

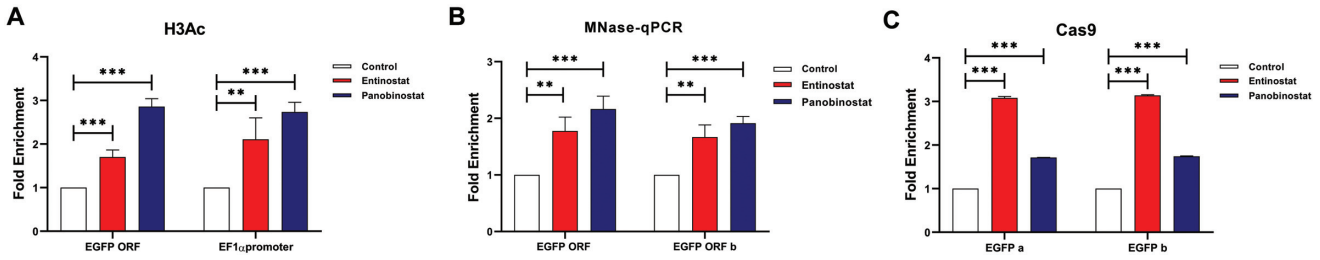

Figure 7. Chromatin immunoprecipitation (ChIP) and qPCR analysis of chromatin state and the binding between Cas9 and targeted DNA with HDAC inhibitors treatment. All CHIP-qPCR and MNAse-qPCR assays were conducted using H27 cell line. (**A**) ChIP-qPCR was performed by using the antibody directly against open chromatin marks Histone3-acetylation (H3Ac). (**B**) MNAse-qPCR was performed by using 5U micrococcal nuclease. (**C**) ChIP-qPCR was performed by using Cas9 antibody directly against the complex of Cas9 protein and the target loci of chromosome. The probed regions were located closely to CRISPR/Cas9 target sequences (−200 bp, +200 bp). Standard positive and negative controls have been described (18).

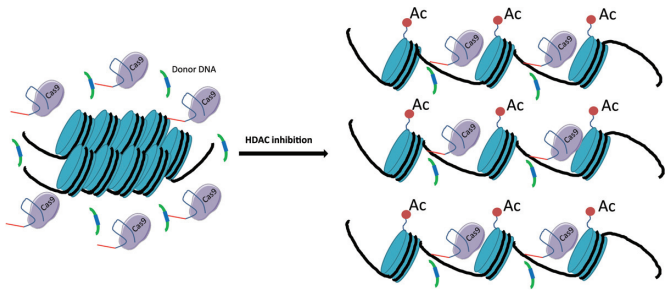

Figure 8. A proposed model of HDAC inhibition and CRISPR/Cas9 mediated gene editing. HDAC inhibition causes unwinding of the target DNA by the addition of acetyl groups to the histones, and thus improving the accessibility of the DNA for gene editing using the CRISPR/CAS9 system. This would enable binding of the nuclease to the desired target sequence and cut the DNA as well as HDR.

tagenesis is mainly depending on Cas9 expression level instead of chromatin state (45). Another study shows that CRISPR/Cas9 cleavage activity is increased by 2.2-fold by changing chromatin state with a TetR-KRAB system in the presence of Dox (18). Thus, different articles have given different answers on how chromatin influences CRISPR/Cas9 targeting from different aspects. Thus, to the best of our knowledge, the underline mechanisms of how Cas9 interacts with chromatinized DNA are still not clear. Therefore, we hypothesized that alteration of chromatin state by HDAC/HAT inhibitors can regulate genome editing by CRISPR/Cas9. Our data support this hypothesis and further show that HDAC1 and HDAC2 play an essential role in improving CRISPR/Cas9 mediated gene editing. Furthermore, we carried out an in-depth investigation to show that downregulation of HDAC1 or 2 activities can open the chromatin and improve the binding between Cas9 proteins and target DNA.

Our data revealed that HDAC inhibition shows remarkable enhancements of HDR events. The extremely low gene knock-in efficiency is one of the main obstacles for gene editing. Our findings contribute to the understanding gene editing by HDR in two aspects. Firstly, our study provides a new practical solution for enhancing gene knock-in with FDA proved HDAC inhibitors. Furthermore, our study suggests that histone acetylation and deacetylation may play an important role in HDR. One possible explanation is that the histone octamer complex around DNA may have strong steric effects for large DNA fragment insertion and integration by HDR. HDAC inhibitors cause unwinding of the target DNA by the addition of acetyl groups to the histones, and thus not only improves the accessibility of the targeted DNA to Cas9 protein, but also to the donor DNA for HDR. This enables binding of desired target sequence to the nuclease as well as to donor DNA. Thus, both knockout and knock-in can be enhanced. In addition, our results also indicate that the HDR events have a positive correlation to the binding of Cas9 protein and targeted DNA (Figures 6B and 7C). Previous study has shown that dissociation of Cas9 protein from double-stranded DNA is ∼6 h which coincides with the HDR time ∼7 h (46,47), we speculate that Cas9 protein may have interactions with double-stranded DNA and facilitate the HDR process during this residence time. Another study shows that opening chromatin by removing histones increases rates of HDR (48). Nonetheless, the precise mechanism of how Cas9 protein interacts with chromatinized DNA remains largely unknown. This needs to be clarified by future studies. Future studies may also need to clarify how Cas9 protein interacts with plain DNA (without histone) and nucleosomal DNA (with histone).

DSBs repair can also be affected by cell cycle arrest, which will eventually influence the gene editing process (49,39). As HDAC inhibitors might affect cell cycle, we investigated the cell cycle changes with the treatment of HDAC inhibitors. We found that Panobinostat (pan-HDAC inhibitor) can increase the proportion of cells in G2/M phase, but we did not observe any cell cycle changes with Entinostat. Thus, we have excluded the gene editing process affected by cell cycle alterations induced by Entinostat. In addition, some of the HDAC or HAT inhibitors can regulate virus transgene expression. Our data has shown that Panobinostat significantly enhance Cas9 protein expression. Similarly, pan-HDAC inhibitors, such as Valproic Acid (VPA), can enhance ZFN expression and cell cycle modulation (50). Also, another study has shown that pan-HDAC inhibition (trichostatin A and vorinostat) can be applied in transient IDLV-mediated ZFN expression modulation. However, we did not observe significant Cas9 expression changes in the condition of HDAC1, HDAC2 and HDAC3 specifically inhibition by Entinostat. Taken together, multiple factors, including G2/M phase cell cycle arrest, virus cellular receptor upregulation, and an increase

in Cas9 expression, may contribute to CRISPR/Cas9 gene editing by Panobinostat. However, our study proved that gene editing efficiency enhanced by Entinostat is not due to those factors, but through changing the chromatin state.

Interestingly, inhibition of HDAC3 attenuated CRISPR/Cas9 gene editing activity, which suggests that HDAC3 played an extraordinary role in the gene editing process. It might be possible to use HDAC3 inhibitors for turning down the activity of Cas9. The first small molecular Cas9 inhibitors have been uncovered recently which can be used for inactivating Cas9 activity (51). Although those inhibitors are with high potency, they might be only effective for SpCas9. However, HDAC3 inhibitors can be used for downregulating the gene editing efficiency through alteration chromatin state regardless of nucleases. HDAC and HAT inhibitors have shown mixed results in different studies and in the treatment of cancers (27). Unlike HDAC1 and HDAC2, which only function in the cell nucleus, HDAC3 is able to shuttle between the nucleus and the cytoplasm (52,53). Inhibition of HDAC3 in the cytoplasm or in the nucleus may have different effects on Cas9 mediated gene editing process. Furthermore, HDAC3 is present at DNA replication forks and inhibition of HDAC3 led to a significant reduction in DNA replication fork velocity (54). Treatment of HDAC3 inhibitor caused inefficient or slowed DNA replication (54). This inefficient DNA replication may affect the DSB repair induced by CRISPR/Cas9 and decrease the gene editing efficiency. Therefore, this unique feature of HDAC3 may be one of the explanations in the mechanism on the decreased gene editing efficiency by HDAC3 inhibition.

Off-target effects are a significant concern for CRISPR/Cas9 technology, especially for clinical use. Although the aim and scope of our study are to enhance CRISPR/Cas9 mediated genome editing by HDAC inhibition, the risk of off-target effects led by those drugs is unwanted. We did not observe any off-targets in these regions with/without treatment of Entinostat. However, we cannot completely rule out any other remaining off-target possibilities due to the limitation of our detection methods. It will be of great interests to further deeply investigate whether HDAC inhibitors might increase off-target effects for future study.

In conclusion, our study provides a practical option for improving gene editing efficiency through chromatin decondensation using HDAC inhibition. Furthermore, our study facilitates a deeper understanding of gene editing process by altering the accessibility of the DNA through histone acetylation and histone deacetylation.

SUPPLEMENTARY DATA

Supplementary Data are available at NAR Online.

ACKNOWLEDGEMENTS

We thank Manuel Gonçalves (Leiden University Medical Center, Department of Cell and Chemical Biology) for providing us with the adenoviral vectors encoding Cas9 and a GFP-targeting gRNA, the human cell lines H27 and HEK.EGFP$^{TetO.KRAB}$ and the plasmids AX03_pgEGFP, AM51_pgNT and AX63_pTHG.donor. We acknowledge Petra E. van der Wouden and Rita Setroikromo for technical support. We thank the Central Flowcytometry Unit of University Medical Center Groningen for providing technical support of flow cytometry. We thank Victor Guryev for the help with analysis of the next-generation sequencing data.

FUNDING

Funding for open access charge: University of Groningen.
Conflict of interest statement. None declared.

REFERENCES

1. Deveau,H., Garneau,J.E. and Moineau,S. (2010) CRISPR/Cas system and its role in phage-bacteria interactions. *Annu. Rev. Microbiol.*, **64**, 475–493.
2. Horvath,P. and Barrangou,R. (2010) CRISPR/Cas, the immune system of bacteria and archaea. *Science*, **327**, 167–170.
3. Bhaya,D., Davison,M. and Barrangou,R. (2011) CRISPR-Cas systems in bacteria and archaea: versatile small RNAs for adaptive defense and regulation. *Annu. Rev. Genet.*, **45**, 273–297.
4. Jinek,M., Chylinski,K., Fonfara,I., Hauer,M., Doudna,J.A. and Charpentier,E. (2012) A programmable dual-RNA-guided DNA endonuclease in adaptive bacterial immunity. *Science*, **337**, 816–821.
5. Cong,L., Ran,F.A., Cox,D., Lin,S., Barretto,R., Habib,N., Hsu,P.D., Wu,X., Jiang,W., Marraffini,L.A. *et al.* (2013) Multiplex genome engineering using CRISPR/Cas systems. *Science*, **339**, 819–823.
6. Luger,K., Mäder,A.W., Richmond,R.K., Sargent,D.F. and Richmond,T.J. (1997) Crystal structure of the nucleosome core particle at 2.8 A resolution. *Nature*, **389**, 251–260.
7. Mali,P., Yang,L., Esvelt,K.M., Aach,J., Guell,M., DiCarlo,J.E., Norville,J.E. and Church,G.M. (2013) RNA-guided human genome engineering via Cas9. *Science*, **339**, 823–826.
8. Liu,B., Saber,A. and Haisma,H.J. (2019) CRISPR/Cas9: a powerful tool for identification of new targets for cancer treatment. *Drug Discov. Today*, **24**, 955–970.
9. Ran,F.A., Hsu,P.D., Lin,C.Y., Gootenberg,J.S., Konermann,S., Trevino,A.E., Scott,D.A., Inoue,A., Matoba,S., Zhang,Y. *et al.* (2013) Double nicking by RNA-guided CRISPR cas9 for enhanced genome editing specificity. *Cell*, **154**, 1380–1389.
10. Ryan,D.E., Taussig,D., Steinfeld,I., Phadnis,S.M., Lunstad,B.D., Singh,M., Vuong,X., Okochi,K.D., McCaffrey,R., Olesiak,M. *et al.* (2018) Improving CRISPR-Cas specificity with chemical modifications in single-guide RNAs. *Nucleic Acids Res.*, **46**, 792–803.
11. Fu,Y., Sander,J.D., Reyon,D., Cascio,V.M. and Joung,J.K. (2014) Improving CRISPR-Cas nuclease specificity using truncated guide RNAs. *Nat. Biotechnol.*, **32**, 279–284.
12. Perez-Pinera,P., Kocak,D.D., Vockley,C.M., Adler,A.F., Kabadi,A.M., Polstein,L.R., Thakore,P.I., Glass,K.A., Ousterout,D.G., Leong,K.W. *et al.* (2013) RNA-guided gene activation by CRISPR-Cas9-based transcription factors. *Nat. Methods*, **10**, 973–976.
13. Abudayyeh,O.O., Gootenberg,J.S., Essletzbichler,P., Han,S., Joung,J., Belanto,J.J., Verdine,V., Cox,D.B.T., Kellner,M.J., Regev,A. *et al.* (2017) RNA targeting with CRISPR-Cas13. *Nature*, **550**, 280–284.
14. Abudayyeh,O.O., Gootenberg,J.S., Konermann,S., Joung,J., Slaymaker,I.M., Cox,D.B.T., Shmakov,S., Makarova,K.S., Semenova,E., Minakhin,L. *et al.* (2016) C2c2 is a single-component programmable RNA-guided RNA-targeting CRISPR effector. *Science*, **353**, aaf5573.
15. Amrani,N., Gao,X.D., Liu,P., Edraki,A., Mir,A., Ibraheim,R., Gupta,A., Sasaki,K.E., Wu,T., Donohoue,P.D. *et al.* (2018) NmeCas9 is an intrinsically high-fidelity genome-editing platform. *Genome Biol.*, **19**, 214.
16. Edraki,A., Mir,A., Ibraheim,R., Gainetdinov,I., Yoon,Y., Song,C.-Q., Cao,Y., Gallant,J., Xue,W., Rivera-Pérez,J.A. *et al.* (2019) A compact, high-accuracy Cas9 with a dinucleotide PAM for in vivo genome editing. *Mol. Cell*, **73**, 714–726.

17. Yarrington,R.M., Verma,S., Schwartz,S., Trautman,J.K. and Carroll,D. (2018) Nucleosomes inhibit target cleavage by CRISPR-Cas9 in vivo. *Proc. Natl. Acad. Sci. U.S.A.*, **115**, 9351–9358.
18. Chen,X., Rinsma,M., Janssen,J.M., Liu,J., Maggio,I. and Gonçalves,M.A.F.V. (2016) Probing the impact of chromatin conformation on genome editing tools. *Nucleic Acids Res.*, **44**, 6482–6492.
19. Uusi-Mäkelä,M.I.E., Barker,H.R., Bäuerlein,C.A., Häkkinen,T., Nykter,M. and Rämet,M. (2018) Chromatin accessibility is associated with CRISPR-Cas9 efficiency in the zebrafish (Danio rerio). *PLoS One*, **13**, e0196238.
20. Isaac,R.S., Jiang,F., Doudna,J.A., Lim,W.A., Narlikar,G.J. and Almeida,R. (2016) Nucleosome breathing and remodeling constrain CRISPR-Cas9 function. *Elife*, **5**, e13450.
21. Verkuijl,S.A. and Rots,M.G. (2019) The influence of eukaryotic chromatin state on CRISPR–Cas9 editing efficiencies. *Curr. Opin. Biotechnol.*, **55**, 68–73.
22. Grunstein,M. (1997) Histone acetylation in chromatin structure and transcription. *Nature*, **389**, 349–352.
23. Eberharter,A. and Becker,P.B. (2002) Histone acetylation: a switch between repressive and permissive chromatin. Second in review series on chromatin dynamics. *EMBO Rep.*, **3**, 224–229.
24. Pinder,J., Salsman,J. and Dellaire,G. (2015) Nuclear domain 'knock-in' screen for the evaluation and identification of small molecule enhancers of CRISPR-based genome editing. *Nucleic Acids Res.*, **43**, 9379–9392.
25. Kwon,D.Y., Zhao,Y.-T., Lamonica,J.M. and Zhou,Z. (2017) Locus-specific histone deacetylation using a synthetic CRISPR-Cas9-based HDAC. *Nat. Commun.*, **8**, 15315.
26. Hilton,I.B., D'Ippolito,A.M., Vockley,C.M., Thakore,P.I., Crawford,G.E., Reddy,T.E. and Gersbach,C.A. (2015) Epigenome editing by a CRISPR-Cas9-based acetyltransferase activates genes from promoters and enhancers. *Nat. Biotechnol.*, **33**, 510–517.
27. Dekker,F.J. and Haisma,H.J. (2009) Histone acetyl transferases as emerging drug targets. *Drug Discov. Today*, **14**, 942–948.
28. Gonçalves,M.A.F.V., van der Velde,I., Knaän-Shanzer,S., Valerio,D. and de Vries,A.A.F. (2004) Stable transduction of large DNA by high-capacity adeno-associated virus/adenovirus hybrid vectors. *Virology*, **321**, 287–296.
29. Janssen,J.M., Chen,X., Liu,J. and Gonçalves,M.A.F.V. (2019) The chromatin structure of CRISPR-Cas9 target DNA controls the balance between mutagenic and homology-directed gene-editing events. *Mol. Ther. - Nucleic Acids*, **16**, 141–154.
30. Hemelaar,S.R., de Boer,P., Chipaux,M., Zuidema,W., Hamoh,T., Martinez,F.P., Nagl,A., Hoogenboom,J.P., Giepmans,B.N.G. and Schirhagl,R. (2017) Nanodiamonds as multi-purpose labels for microscopy. *Sci. Rep.*, **7**, 720.
31. Cao,F., Zwinderman,M., van Merkerk,R., Ettema,P., Quax,W. and Dekker,F.J. (2019) Inhibitory selectivity among class I HDACs has a major impact on inflammatory gene expression in macrophages. *Eur. J. Med. Chem.*, **177**, 457–466.
32. Maggio,I., Holkers,M., Liu,J., Janssen,J.M., Chen,X. and Gonçalves,M.A.F.V. (2014) Adenoviral vector delivery of RNA-guided CRISPR/Cas9 nuclease complexes induces targeted mutagenesis in a diverse array of human cells. *Sci. Rep.*, **4**, 5105.
33. Janssen,J.M., Liu,J., Skokan,J., Gonçalves,M.A.F.V. and de Vries,A.A.F. (2013) Development of an AdEasy-based system to produce first- and second-generation adenoviral vectors with tropism for CAR- or CD46-positive cells. *J. Gene Med.*, **15**, 1–11.
34. Holkers,M., Maggio,I., Henriques,S.F.D., Janssen,J.M., Cathomen,T. and Gonçalves,M.A.F.V. (2014) Adenoviral vector DNA for accurate genome editing with engineered nucleases. *Nat. Methods*, **11**, 1051–1057.
35. Alemany,R. and Curiel,D.T. (2001) CAR-binding ablation does not change biodistribution and toxicity of adenoviral vectors. *Gene Ther.*, **8**, 1347–1353.
36. Bae,S., Park,J. and Kim,J.-S. (2014) Cas-OFFinder: a fast and versatile algorithm that searches for potential off-target sites of Cas9 RNA-guided endonucleases. *Bioinformatics*, **30**, 1473–1475.
37. Bornelöv,S., Reynolds,N., Xenophontos,M., Gharbi,S., Johnstone,E., Floyd,R., Ralser,M., Signolet,J., Loos,R., Dietmann,S. *et al.* (2018) The nucleosome remodeling and deacetylation complex modulates chromatin structure at sites of active transcription to fine-tune gene expression. *Mol. Cell*, **71**, 56–72.
38. Infante,J.J., Law,G.L. and Young,E.T. (2012) Analysis of nucleosome positioning using a nucleosome-scanning assay. *Methods Mol. Biol.*, **833**, 63–87.
39. Haapaniemi,E., Botla,S., Persson,J., Schmierer,B. and Taipale,J. (2018) CRISPR–Cas9 genome editing induces a p53-mediated DNA damage response. *Nat. Med.*, **24**, 927–930.
40. Tate,C.R., Rhodes,L.V, Segar,H.C., Driver,J.L., Pounder,F.N., Burow,M.E. and Collins-Burow,B.M. (2012) Targeting triple-negative breast cancer cells with the histone deacetylase inhibitor panobinostat. *Breast Cancer Res.*, **14**, R79.
41. Butler,M. (1999) Cell counting and viability measurements. In: *Animal Cell Biotechnology*. Humana Press, New Jersey, pp. 131–144.
42. Janssen,J.M., Chen,X., Liu,J. and Gonçalves,M.A.F.V. (2019) The chromatin structure of CRISPR-Cas9 target DNA controls the balance between mutagenic and homology-directed gene-editing events. *Mol. Ther. Nucleic Acids*, **16**, 141–154.
43. Mieczkowski,J., Cook,A., Bowman,S.K., Mueller,B., Alver,B.H., Kundu,S., Deaton,A.M., Urban,J.A., Larschan,E., Park,P.J. *et al.* (2016) MNase titration reveals differences between nucleosome occupancy and chromatin accessibility. *Nat. Commun.*, **7**, 11485.
44. Chen,X., Liu,J., Janssen,J.M. and Gonçalves,M.A.F.V. (2017) The Chromatin Structure Differentially impacts high-specificity CRISPR-Cas9 nuclease strategies. *Mol. Ther. Nucleic Acids*, **8**, 558–563.
45. PLOS Biology Staff (2019) Correction: Heterochromatin delays CRISPR-Cas9 mutagenesis but does not influence the outcome of mutagenic DNA repair. *PLoS Biol.*, **17**, e3000160.
46. Richardson,C.D., Ray,G.J., DeWitt,M.A., Curie,G.L. and Corn,J.E. (2016) Enhancing homology-directed genome editing by catalytically active and inactive CRISPR-Cas9 using asymmetric donor DNA. *Nat. Biotechnol.*, **34**, 339–344.
47. Mao,Z., Bozzella,M., Seluanov,A. and Gorbunova,V. (2008) Comparison of nonhomologous end joining and homologous recombination in human cells. *DNA Repair (Amst).*, **7**, 1765–1771.
48. Hauer,M.H., Seeber,A., Singh,V., Thierry,R., Sack,R., Amitai,A., Kryzhanovska,M., Eglinger,J., Holcman,D., Owen-Hughes,T. *et al.* (2017) Histone degradation in response to DNA damage enhances chromatin dynamics and recombination rates. *Nat. Struct. Mol. Biol.*, **24**, 99–107.
49. Ihry,R.J., Worringer,K.A., Salick,M.R., Frias,E., Ho,D., Theriault,K., Kommineni,S., Chen,J., Sondey,M., Ye,C. *et al.* (2018) p53 inhibits CRISPR–Cas9 engineering in human pluripotent stem cells. *Nat. Med.*, **24**, 939–946.
50. Joglekar,A. V, Stein,L., Ho,M., Hoban,M.D., Hollis,R.P. and Kohn,D.B. (2014) Dissecting the mechanism of histone deacetylase inhibitors to enhance the activity of zinc finger nucleases delivered by integrase-defective lentiviral vectors. *Hum. Gene Ther.*, **25**, 599–608.
51. Maji,B., Gangopadhyay,S.A., Lee,M., Shi,M., Wu,P., Heler,R., Mok,B., Lim,D., Siriwardena,S.U., Paul,B. *et al.* (2019) A high-throughput platform to identify small-molecule inhibitors of CRISPR-Cas9. *Cell*, **177**, 1067–1079.
52. Longworth,M.S. and Laimins,L.A. (2006) Histone deacetylase 3 localizes to the plasma membrane and is a substrate of Src. *Oncogene*, **25**, 4495–4500.
53. Yang,W.-M., Tsai,S.-C., Wen,Y.-D., Fejér,G. and Seto,E. (2002) Functional domains of histone deacetylase-3. *J. Biol. Chem.*, **277**, 9447–9454.
54. Wells,C.E., Bhaskara,S., Stengel,K.R., Zhao,Y., Sirbu,B., Chagot,B., Cortez,D., Khabele,D., Chazin,W.J., Cooper,A. *et al.* (2013) Inhibition of histone deacetylase 3 causes replication stress in cutaneous T cell lymphoma. *PLoS One*, **8**, e68915.